JACS
JOURNAL OF THE AMERICAN CHEMICAL SOCIETY

Communication

pubs.acs.org/JACS

Sensitive Biological Detection with a Soluble and Stable Polymeric Paramagnetic Nanocluster

Benjamin Kim, Anne H. Schmieder , Allen J. Stacy, Todd A. Williams, and Dipanjan Pan*

C-TRAIN and Division of Cardiology, Washington University School of Medicine, 4320 Forest Park Avenue, Saint Louis, Missouri 63108, United States

Supporting Information

ABSTRACT: We describe the design, synthesis, and biological characterization of manganese oxocluster-based "single molecule magnets (SMMs)". We demonstrate that polymeric micellar nanoparticles can serve as a carrier and help to stabilize delicate SMM molecules from breaking down easily and thus prevent their property loss. Concentrating thousands of Mn-clusters per micelle provided a high ionic and per-particle relaxivity allowing sensitive MR imaging *in vivo*. This reports one of the earliest examples of *in vivo* imaging of a rationally designed polymeric micelle that features SMM.

Molecular nanomagnets are organic molecules with a single or multiple metal ions having unpaired electrons in their outer orbitals.[1] These molecules are often referred as "single molecule magnets" (SMMs) as they show superparamagnetic behavior under a certain blocking temperature at the molecular scale exhibiting magnetic properties of purely molecular origin. The prerequisites for SMM behavior are (i) a very high spin state and (ii) a large magnetic anisotropy.[2] Lis et al. described one of the earlier examples of SMM comprising a cluster of 12 manganese ions with acetate ligands, often called Mn_{12}-acetate $[[Mn_{III/IV12}O_{12}(CH_3CO_2)_{16}(H_2O)_4]$.[3] In this dodecanuclear mixed-valence manganese carboxylate cluster eight of the manganese ions are in the +3 oxidation state (spin $S = 2$), and four are in the +4 state (spin $S = {}^3/_2$). Such clusters are thus able to obtain a magnetically coupled large ground state of $S = 10$ and are responsible for many frequency-dependent unfamiliar magnetic relaxation effects, properties,[4,5] and application.[6−10]

Vasovist (MS-325), which is a gadolinium-based (gadofosveset trisodium) agent, has been approved for peripheral vascular and coronary artery disease. However, in light of the recent FDA warning about an association between gadolinium (Gd)-based contrast agents and nephrogenic systemic fibrosis (NSF), the use of the lanthanide Gd is now more regulated.[11] The intrinsic property of Mn_{12} is somewhere between paramagnetic complexes and superparamagnetic nanoparticles. Recently, they have been explored as contrast agents for biological imaging. However, their poor stability and solubility in water are major drawbacks for successful translation to preclinical applications. A few approaches were proposed including binding the clusters to polystyrene beads and an emulsion-assisted self-assembly method for dispersing stearic acid-modified Mn_{12}.[12] While these were viable approaches to use SMM as a T2-weighted (darkening contrast) MRI agent, a more biocompatible, robust methodology is required to use it as a T1-weighted agent (brightening contrast) to diagnose vascular disease. We hypothesized that the induced magnetic moment of Mn_{12} clusters in the applied field would accelerate the relaxation of surrounding water protons. Clearly, a more biocompatible approach is the unmet need by restricting the agent within a size range of <20 nm to impede in the bloodstream for delayed extravascular leakage and prolonged retention. This will enable the rapid acquisition of high-resolution MRAs using clinical MRI machines. Toward this aim, we developed and characterized a new "soft" nanomagnet comprising the Mn_{12} and a well-defined polymeric micellar nanoparticle (Poly-SMM) for sensitive MRI detectability. This strategy offers several advances over the existing reports, particularly the poor inherent aqueous stability to address the inherent insolubility issues with the parent Mn_{12} molecules. Our objective was to develop a platform comprising multiple copies (in hundreds) of Mn_{12} clusters, which presented the metal ions directly on the surface for increased interaction with surrounding water. The shortened relaxation of the surrounding water protons provides a T1-weighted contrast agent. For the carrier nanoparticles, a stable polymeric system with a sub-20-nm particle size for eventual biomedical application in extravascular imaging and drug delivery was developed. Our approach followed a co-self assembly of amphiphilic diblock copolymer and a well-known surfactant to restrict the particle sizes within 20 nm.

Mn_{12}-acetate was synthesized in a way similar to the method of Lis et al.[3] Briefly, $Mn(CH_3CO_2)_2{\cdot}4H_2O$ was dissolved in a mixture of 60% acetic acid and water. To this, finely ground $KMnO_4$ was added in small amounts over the course of about 2 min until dissolved. The final solution was removed from the stir plate and allowed to remain undisturbed for 3 days to observe the crystalline growth of long black rectangular rods. For the synthesis of polymeric micelles, an amphiphilic diblock-*co*-polymer polystyrene-*b*-poly(acrylic acid)[13] (PS_8-*b*-PAA_{400}, Mn × 10^{-3}: 0.8-*b*-29.3 polydispersity index: PDI = 1.18, 0.33 μmol, 6.0 mg, 0.5 mol %) was co-self assembled with polyoxyethylene (20) sorbitan monooleate (polymer: polysorbate = 6:1). The mixture was briefly bath sonicated at ambient temperature for 2 min until a transparent suspension was achieved. The formation of the micelles was confirmed by dynamic light scattering (DLS) measurement, which revealed a particle size of 16 ± 4 nm with polydispersity 0.021. Zeta

Received: April 26, 2012
Published: June 6, 2012

   dx.doi.org/10.1021/ja3040366 | *J. Am. Chem. Soc.* 2012, 134, 10377−10380

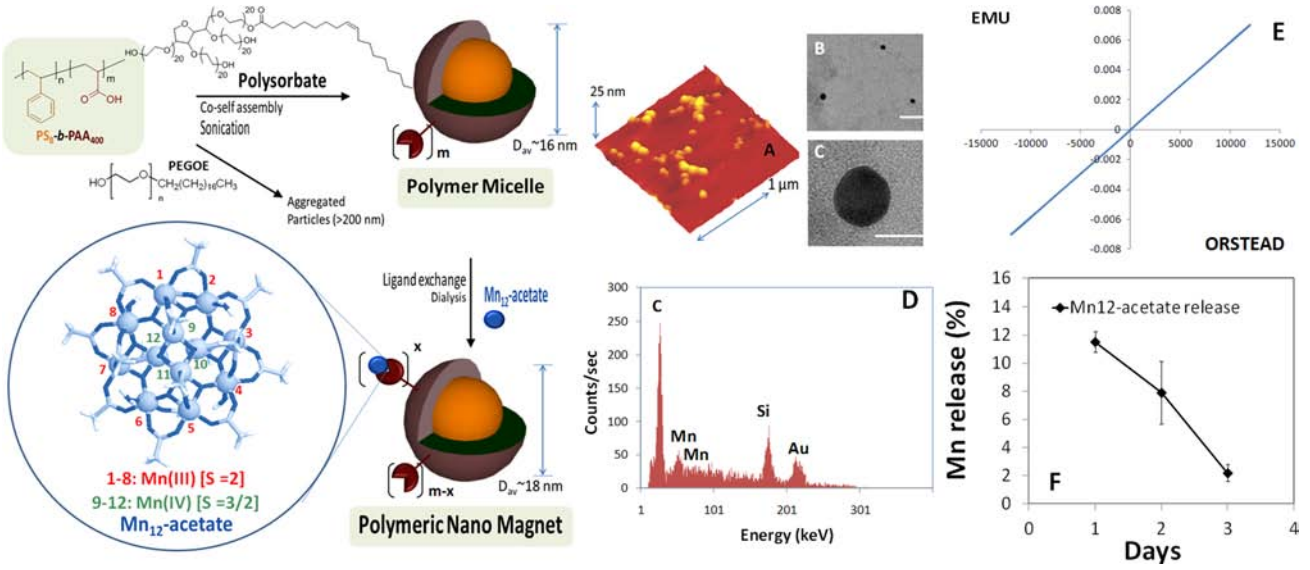

Figure 1. Synthesis and characterization of Poly-SMM. (i) Co-self assembly of amphiphilic diblock copolymer (PS-*b*-PAA) and sorbitan monooleate, sonication, 25 °C, 2 min; (ii) Mn_{12}-acetate; dialysis 10 kDa cellulosic membrane, nanopure water (0.2 μM). (A) AFM image of Poly-SMM drop deposited over freshly cleaved mica; (B) TEM images of Poly-SMM (scale = 100 nm); (C) an enhanced image of a single nanoparticle (scale = 20 nm); (D) EDX spectrum of Poly-SMM; (E) VSM magnetization and hysteresis graph; (F) dissolution of Mn_{12}-acetate from Poly-SMM over three days against infinite sink of water.

(electrophoretic potential) values ($\zeta = -12 \pm 3$ mV) were negative, confirming a predominant occupancy of the surface by the carboxylic acid groups of the hydrophilic polyacrylate segment of the amphiphilic copolymer. Polysorbate was purposefully chosen as a cosurfactant to impart stability to the micelles after the attachment of the oxoclusters and to restrict the particle diameter within 20 nm with low polydispersity. From an initial 1:6 ratio of block copolymer and polysorbate concentrations, we varied the ratio to optimize the concentration of components in the mixture (Supporting Information [SI] Figure 1S). Our attempt to use a different cosurfactant as polyethylene glycol octadecyl ether (PEGOE) resulted in aggregated particles with particle sizes over 200 nm. (SI Figure 2S) We presume that the attachment of Mn_{12}-acetate to the polymeric micelles was driven by ligand substitution reactions owing to the presence of the more acidic carboxylates of PAA ($pK_a \approx 4$) [Mn_{12}acetate + $16RCO_2H \rightarrow (Mn_{12}O_{12}(O_2CR)_{16}(H_2O)_4 + 16MeCO_2$; R = acrylic]. The ligand exchange reaction did not greatly alter the hydrodynamic diameter of the post-conjugated micelles. Unbound Mn clusters were removed by exhaustive dialysis against an infinite sink of water using a 10 kDa MWCO cellulosic membrane. The particles were characterized by transmission electron microscopy (TEM), atomic force microscopy (AFM), scanning electron microscopy (SEM), energy dispersive X-ray spectroscopy (EDX), and inductively coupled plasma resonance-optical emission spectroscopy (ICP-OES). DLS measurements revealed the number-averaged hydrodynamic diameter as 17 ± 4 nm with low electrophoretic potential values ($\zeta = -10 \pm 5$ mV). As evident from the polydispersity indexes (PDI: 0.17), these particles were produced with narrow distribution. The anhydrous state properties were determined by AFM (Figure 1A) and TEM (Figure 1B–C) analyses by drop depositing the aqueous suspension of the Poly-SMM over a glass slide. The particle height was calculated to be 14 ± 6 nm. UV–vis spectroscopy confirmed the absorbencies at ~520 nm, corresponding to the presence of multiple Mn_{12} atoms in oxo clusters and charge transfers from the inner Mn ions toward the outer ones. The concentration of manganese was analytically determined by ICP-OES. On the basis of an average of three formulations, the concentration of undiluted Poly-SMM was measured to be 4.7 mg/L, which equates to ~3000 Mn/particle nominally. EDX spectroscopy (Figure 1D) further confirmed the presence of Mn, as evident from the occurrence of primary and secondary emission lines at 0.637 and 0.649 keV, respectively. The magnetic susceptibility measurements described by a vibrating sample magnetometer (VSM) revealed that the predominant phase of the material is paramagnetic in nature. (Figure 1E) These uniquely constructed polymeric nanoparticles possess long shelf-life stability and retain the particle integrity for their further exploration in preclinical studies. The stability and stringency of Mn_{12} liagnds associated with the micelles were studied in a dissolution experiment. The release of the Mn complex was examined by UV spectroscopy at ~520 nm wavelength range and reveals a less than ~19% total release over 3 days against an infinite sink, indicating a nominal loading efficiency of 81–83% with good retention in dissolution at 37 °C. The majority of the Mn was released during the first (11 ± 1%) and second (7 ± 2%) day of dissolution. Time-dependent stability of the particles at ambient temperature and within a physiological pH range 6–8 was studied, and a minor variance was confirmed on the basis of light-scattering and electrophoretic potential measurements. To assess the blood and serum stability, a 'blood smear' assay was performed to study morphological changes in lymphocytes and blood clumping using conventional light microscopy under high-power field. As represented in Figure 2(A,B), no significant clumping or morphological alterations were observed in rodent blood treated with Poly-SMM (blood/NP = 4:1) (experimental details in the SI).

As discussed above, Poly-SMMs were purified by exhaustive dialysis against an infinite sink of water prior to characterizing magnetic resonance (MR) properties. The MR properties of serially diluted Poly-SMMs were characterized in aqueous

dx.doi.org/10.1021/ja3040366 | J. Am. Chem. Soc. 2012, 134, 10377–10380

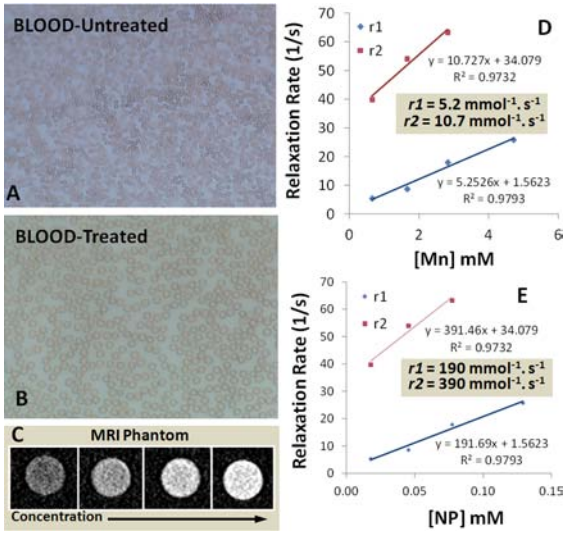

Figure 2. Optical microscopy images of 'blood smear' (A) untreated (magnification: 20×) and (B) treated with Poly-SMM (magnification: 40×). (C) Image shows the T1-weighted MRI of the contrast agent diluted in water from lowest concentration tested to highest (as shown with arrow); relaxivity measurements of Poly-SMM: relaxivities, r_1 and r_2, are calculated from the measured relaxation rates as a function of Poly-SMM concentration. The graphs are the data for longitudinal relaxation rate (R1) and transverse relaxation rate (R2) at 1.5 T based on [Mn] (D) and [NP] (E).

suspension. Four dilutions of the particles were prepared in microcentrifuge tubes at approximately 1:0, 1:2, 1:4, and 1:8 Poly-SMMs/ultrapure water (0.2 μM), corresponding to 4.7, 2.8, 1.6, and 0.6 mM Mn. The nominal nanoparticle concentration was calculated from particle size determined by laser light scattering, and the total volume of Mn cluster incorporated into Poly-SMMs was adjusted for loss of metal during dialysis. The dilutions were scanned at room temperature on clinical MRI scanners (1.5 T) with a transmit-and-receive birdcage head coil (Achieva, Philips Healthcare) to measure relaxation rates, R1 and R2. A single slice inversion recovery sequence (i.e., the Look–Locker technique)[14] was employed to calculate the ionic (per millimole of Mn) and particulate (per millimole Poly SMMs) r_1 relaxivities at 1.5 T (resolution = 0.7 × 0.7 × 3 mm^3, 30 samples of the inversion recovery signal starting at 17 ms and spaced at 7 ms, with 10° sampling flip angle, TE = 1.9 ms, TR = 4.14 s, four averages). Similarly, r_2 relaxivity was measured using a multi-echo–spin–echo technique, resolution = 0.9 × 0.9 × 3 mm^3, 20 echoes at 4.4 ms intervals, TR = 541 ms, four averages). The relaxivities (mean ± std error) for the poly-SMM based on Mn concentrations are r_1 = 5.2 ± 0.12 mM^{-1} s^{-1} [Mn] and r_2 = 10.7 ± 0.24 mM^{-1} s^{-1} [Mn] at 1.5 T. The ionic relaxivity values of poly-SMM were found to be similar to those of commercially available gadolinium-based contrast agents (e.g., Magnevist).[15] It is worth mentioning that the ionic relaxivity (r_1) of Poly-SMM is much higher than those of previously reported procedures.[6,7] Interestingly, a solution of Mn_{12}-acetate in acetic acid (excess) produced a r_1 = 3.0 mM^{-1} s^{-1}, which is lower than that of Poly-SMMs. Particulate relaxivities were also calculated as r_1 = 192 ± 20 mM^{-1} s^{-1} [Poly-SMMs] and r_2 = 390 ± 65 mM^{-1} s^{-1} [Poly-SMMs] for 1.5 T (Figure 2).

In vivo MRI imaging was performed in a rat model (n = 3) to evaluate contrast using an intravenous (IV) dose (tail vein) of 2 mL/kg, 0.28 mmol of Mn/kg. MR imaging was performed pre- and post-intravenous administration of Poly-SMM into each rat. The MRI signal enhancement of major clearance organs was monitored over a period of 2.5 h. (Figure 3) The significant

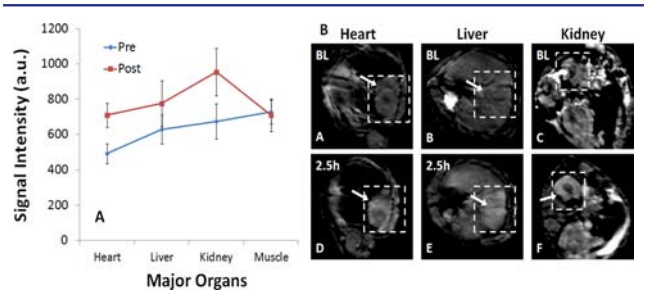

Figure 3. *In vivo* MR imaging of Poly-SMM. (A) Signal intensity of the major organs before and after the administration of Poly-SMMs. (B) MRI images of major organs at baseline (A–C) and 2.5 h (D–F) at 1.5 T, indicating superior delineation after Poly-SMM administration.

enhancement of the MR signal of the major organs including the liver, heart, and kidney was observed. At 2.5 h after Poly-SMM injection, the MR signals corresponding to heart, liver, and kidney were respectively enhanced by 144%, 123%, and 141%. The enhancement of signal in the heart even after 2 h indicates that these particles may presumably have a long circulatory half-life and can be used eventually for coronary imaging. Furthermore, in a preliminary biodistribution studies, the parent particles incorporated with a water-soluble near-infrared dye (ADS832WS, λ_{ex} = 824 nm, 1.90 × 10^5 L mol^{-1} cm^{-1}) was probed *in vivo* with optical imaging (IVIS). Bio-d of the polymeric nanoparticles was determined at 2 h and 24 h post-IV injection (1 mL/kg). Liver was found to be the predominant organ of the micelle accumulation as was obvious from the measured fluorescence intensity. The other major clearance organs were kidney, lymph node, and spleen. (SI Figure 3S) The superior delineation of the reticuloendothelial (RES) organs (liver, spleen, etc.) suggested that the particles apparently had distributed into major clearance organs, typical of nanoparticulate agents. More in-depth clearance and PK studies will be required to fully understand their *in vivo* behavior.

In conclusion, we have taken a rational approach to polymeric nanomagnet design for better sensitivity and improved inherent properties for preclinical application. A fast synthetic route is chosen to co-self assemble amphiphilic polymers to produce sub-20-nm-sized micelles presenting carboxylic acid groups on the surface. Mn_{12}-acetate, a well-studied single-magnet molecule, was chosen to embellish the polymeric shell by a ligand-exchange reaction mechanism. *In vitro* MRI studies revealed that these particles offered higher T1 relaxivity in comparison to naked Mn_{12}-acetate and were also more efficacious than the recently reported approaches. Finally, in a preliminary *in vivo* study we demonstrated that these particles can successfully be used for biological imaging in living subjects. Although more in-depth studies are warranted to fully understand the temperature-dependent magnetic susceptibility and the effect of cosurfactant in this polymeric system, to the best of our knowledge, we report the first *in vivo* imaging of a rationally designed polymeric particle that incorporates 'single molecule magnets'.

dx.doi.org/10.1021/ja3040366 | J. Am. Chem. Soc. 2012, 134, 10377–10380

■ ASSOCIATED CONTENT

Supporting Information

Description of experimental methods and analytical measurements. This material is available free of charge via the Internet at http://pubs.acs.org.

■ AUTHOR INFORMATION

Corresponding Author

dipanjan@wustl.edu

Notes

The authors declare no competing financial interest.

■ ACKNOWLEDGMENTS

This research was supported by grants from the AHA (0835426N and 11IRG5690011), NIH (R01CA154737, R01HL094470, R01NS059302), and NCI (U54CA119342). We are thankful to Profs G. M. Lanza and S. A. Wickline for their suggestions and K. Nelson (NRF) for TEM and AFM experiments.

■ REFERENCES

(1) (a) Yang, P., Ed. *Chemistry of Nanostructured Materials*; World Scientific Publishing: Hong Kong, 2003. (b) Cornia, A.; Mannini, M.; Sainctavit, P.; Sessoli, R. *Chem Soc Rev.* **2011**, *40*, 3076−3091. (c) Glaser, T. *Chem. Commun. (Camb.)* **2011**, *47*, 116−30. (d) Gatteschi, D. *Alloys Compd.* **2001**, *317*, 8−12. (e) Hendrickson, D. N.; Christou, G.; Ishimoto, H.; Yoo, J.; Brechin, E. K.; Yamaguchi, A.; Rumberger, E. M.; Aubin, S. M. J.; Sun, Z.; Aromi, G. *Mol. Cryst. Liq. Cryst.* **2002**, *376*, 301−313. (f) Sessoli, R.; Gatteschi, D.; Caneschi, A.; Novak, M. *Nature* **1993**, *365*, 141.

(2) (a) Milios, C. J.; Vinslava, A.; Wernsdorfer, W.; Moggach, S.; Parsons, S.; Perlepes, S. P.; Christou, G.; Brechin, E. K. *J. Am. Chem. Soc.* **2007**, *129*, 2754. (b) Cavallini, M.; Facchini, M.; Albonetti, C.; Biscarini, F. *Phys. Chem. Chem. Phys.* **2008**, *10*, 784.

(3) Lis, T. *Acta Crystallogr., Sect. B* **1980**, *36*, 2042.

(4) Caneschi, A.; Gatteschi, D.; Sessoli, R.; Barra, A. L.; Brunel, L. C.; Guillot, M. *J. Am. Chem. Soc.* **1991**, *113*, 5873−5874.

(5) Sessoli, R.; Tsai, H.-L.; Schake, A. R.; Wang, S.; Vincent, J. B.; Folting, K.; Gatteschi, D.; Christou, G.; Hendrickson, D. N. *J. Am. Chem. Soc.* **1993**, *115*, 1804−1816.

(6) Fang, X.; Kögerler, P.; Speldrich, M.; Schilder, H.; Luban, M. *Chem. Commun. (Camb.)* **2012**, *48*, 1218−20.

(7) Gatteschi, D.; Sessoli, R.; Cornia, A. *Chem. Commun.* **2000**, 725−732.

(8) Gonidec, M.; Biagi, R.; Corradini, V.; Moro, F.; De Renzi, V.; del Pennino, U.; Summa, D.; Muccioli, L.; Zannoni, C.; Amabilino, D. B.; Veciana, J. *J. Am. Chem. Soc.* **2011**, *133*, 6603−6612.

(9) (a) Mills, D. P.; Moro, F.; McMaster, J.; van Slageren, J.; Lewis, W.; Blake, A. J.; Liddle, S. T. *Nature Chem.* **2011**, *3*, 454−60. (b) Inglis, R.; Dalgarno, S. J.; Brechin, E. K. *Dalton Trans.* **2010**, *39*, 4826−4831.

(10) Gatteschi, D.; Sessoli, R. *Angew Chem., Int. Ed.* **2003**, *42*, 268.

(11) Kuo, P. H.; Kanal, M.; Abu-Alfa, A. K.; Cowper, S. E. *Radiology* **2007**, *242*, 647−649.

(12) (a) Mertzman, J. E.; Kar, S.; Lofland, S.; Fleming, T.; Keuren, E. V.; Tong, Y. Y. *Chem. Commun.* **2009**, 788−790. (b) Yinglin, W.; Wen, L.; Shengyan, Z.; Daliang, K.; Haishan, Y.; Lixin, W. *Chem. Commun. (Camb.)* **2011**, *47*, 3541−3543.

(13) Pan, D.; Williams, T. A.; Senpan, A.; Allen, J. S.; Scott, M. J.; Gaffney, P. J.; Wickline, S. A.; Lanza, G. M. *J. Am. Chem. Soc.* **2009**, *131*, 15522−7.

(14) Look, D. C.; Locker, D. R. *Rev. Sci. Instrum.* **1970**, *41* (621), 7.

(15) Pintaske, J.; Martirosian, P.; Graf, H.; Erb, G.; Lodemann, K. P.; Claussen, C. D.; Schick, F. *Invest. Radiol.* **2006**, *41*, 213−21.